



Wound healing activity of aqueous dispersion of fullerene C₆₀ produced by “green technology”

N.N. Shershakova, PhD^{a,*}, S.M. Andreev, PhD^a, A.A. Tomchuk, MSc^b, E.A. Makarova, MSc^a, A.A. Nikonova, PhD^a, E.A. Turetskiy, PhD^a, O.A. Petukhova, MSc^a, O.Y. Kamyshnikov, MSc^a, O.I. Ivankov, PhD^{b,c}, O.A. Kyzyma, DSc^d, O.V. Tomchuk, PhD^{b,d}, M.V. Avdeev, DSc^b, A.S. Dvornikov, DSc, MD^f, D.A. Kudlay, DSc, MD^{a,e}, M.R. Khaitov, DSc, MD^{a,f}

^aNRC Institute of Immunology FMBA of Russia, Kashirskoe shosse, 24, Moscow 115522, Russian Federation

^bInternational intergovernmental organization Joint Institute for Nuclear Research, st. Joliot-Curie, 6, Dubna, Moscow Region 141980, Russian Federation

^cMoscow Institute of Physics and Technology, 9 Institutskiy per., Dolgoprudny, Moscow Region 141701, Russian Federation

^dTaras Shevchenko National University of Kyiv, 64/13, Volodymyrska Street, Kyiv 0160, Ukraine

^eI.M. Sechenov First Moscow State Medical University (Sechenov University), 8-2 Trubetskaya str., Moscow 119991, Russian Federation

^fPirogov Russian National Research Medical University, 1 Ostrovityanov St., Moscow 119997, Russian Federation

Revised 13 August 2022

Abstract

In addition to exhibited antioxidant and anti-inflammatory activity, fullerene C₆₀ is a promising wound healing agent. An important stage in the production of fullerene-based ointments is the stability of the aqueous fullerene dispersion (AFD) with minimum size of colloidal fullerene aggregates and sufficiently high concentration. To achieve these parameters tangential flow filtration of fullerene C₆₀ was used (“green technology”).

As estimated by small-angle neutron scattering and dynamic light scattering purified AFDs with narrow-size distribution nanoclusters have a size of 6 nm and are assembled into agglomerates which reach a size of 150 nm.

The ability of the AFD to exhibit regenerative activity was studied using the animal wound model. This study shows for the first time that the fullerene-based composition stimulates the healing of wounds of various origins. We assume that the mechanism of the AFD wound-healing activity is associated with the aryl hydrocarbon receptor and macrophages activity.

© 2022 Elsevier Inc. All rights reserved.

Keywords: Fullerene C₆₀; Green technology AFD; Regenerative activity; Small-angle scattering; Dynamic light scattering; AhR

Background

Skin wound healing is a complex process with different cell types and multiple regulatory factors involved. The effective treatment is hindered by concomitant aggravating disorders (diabetes, hypertension, vascular, autoimmune diseases and bacterial superinfections).¹ Therefore, a wound healing presents a serious medical problem and requires development of safe and effective therapeutic agents. The basis of the available preparations for wound healing are adsorbents, anti-inflammatory components, antibiotics or dexapanthenol (Baneocin, Bepanten,

Panthenol, Ichthammol ointment, Zinc oxide ointment, Cicaplast, etc.), which stimulates regeneration processes. Number of studies demonstrated that reactive oxide forms (ROS), as nitric oxide and hydrogen peroxide, are important factors in wound healing process.

Excess of ROS generated internally or externally can damage key cell components, influence intracellular signaling and balance between oxidants and antioxidants in the tissue which is necessary for a successful healing process.^{2–4} Thus, the antioxidant-based drugs prospect is the relief of oxidative stress which contributes to elimination of the inflammation and the earliest onset of the regeneration.

In addition, different types of scar tissue can occur during healing processes. Scars can restrict movements, cause pain,

* Corresponding author.

E-mail address: nn.shershakova@nrcii.ru (N.N. Shershakova).

itchiness, as well as physiological stress in the case when skin scars remain visible and cannot be hidden by clothing or makeup; that can have a serious impact on self-esteem and quality of life. The reduction of scarring is still a challenge. Despite a variety of scar treatments available their effectiveness is rather limited. The global scar treatment market size stood at \$19.6 billion in 2019 and is expected to grow by 11.5 % in the next decade.⁵

Fullerene C₆₀ is a molecular carbon form with cage spheroidal structure possessed strong antioxidant activity. It is known that water-soluble forms of fullerene C₆₀ exhibits multiple biological effects including antiviral, anti-inflammatory, anti-allergic and regenerative properties.^{6–12} Certain covalent derivatives of fullerene C₆₀ have been shown to accelerate wound healing in a mouse model of skin irritation and prevent infiltration of inflammatory cells, although their mechanism of action remains unknown.¹³ Recent study describes the efficient regeneration of lung epithelial cells damaged by oxidative stress after treatment with fullerene C₆₀ dispersion (particles of 170–200 nm size in buffer with fetal serum), and authors suggested that this fullerene-based formulation may be active in the treatment and prevention of acute respiratory distress syndrome associated with COVID-19.¹⁴

The water-soluble fullerene C₆₀ in form of non-covalent complex with polyvinylpyrrolidone is also known as a free radical scavenger. It significantly inhibited the production of proinflammatory cytokines induced by TNF- α in synovial fibroblasts, infiltrating lymphocytes, and macrophages in the rat model of arthritis.¹⁵ The decrease in TNF- α , IL-6, IL-1 after treatment with hydroxylated fullerene was observed on *in vitro* model of oxidative stress in mouse peritoneal macrophage culture with overexpression of TLR2 receptors.¹⁶ Certain fullerene derivatives have been able to prevent the development of inflammation and edema of mice ear after administration of phorbol-myristate-acetate (mouse model of delayed-type hypersensitivity reaction).¹⁷

The fullerene C₆₀ potential therapeutic utility becomes possible due to its ability to form stable aqueous dispersions of nanoparticles. Common method for synthesis of aqueous fullerene C₆₀ dispersion is solvent exchange (toluol)/ultrasonic.^{18,19} However, the limiting concentrations of transparent AFDs obtained by this method remained in the range of 130–200 mg of C₆₀/L.²⁰

In this study we synthesized the aqueous fullerene C₆₀ dispersion by developed diafiltration-based technology.²¹ Our technique allows purifying AFDs with concentration of 1 g/L in highly stable form, or up to 2–3 g/L, but with lower stability.

The diafiltration technology is a tangential flow filtration (TFF) based method that has a great advantage due to the biocompatible technology that allows obtaining concentrated dispersions and scaling up the process. In addition, the availability of more concentrated AFD allows to apply advanced scattering methods (*e.g.*, small-angle scattering²²) for more efficient determination of the structural organization of the fullerene solutions.

As the fullerene C₆₀ dispersion is an aqueous colloidal system containing molecular aggregates (nanoparticles) its temporal stability depends on several factors, such as the structural sta-

bility of nanoparticles, surface charge, ionic strength and the presence of stabilizers. Consequently, the stability of AFDs is limited in the presence of electrolytes (as in physiological environment). To increase the concentration and the stability of C₆₀ nanoparticles in the AFD, the biocompatible nonionic surfactant usually used. However, the structural organization of AFD obtained by this method has not been specifically studied.

In this study we aimed to analyze the structure of the fullerene C₆₀ stabilized aqueous dispersion produced by diafiltration technology and to evaluate its biological activity. Various physicochemical methods are used to characterize the structure of dispersion.²³ The structure analysis was performed by small angle X-ray scattering (SAXS), small-angle neutron scattering (SANS), dynamic light scattering (DLS) and ultraviolet–visible (UV–Vis) absorption spectroscopy with assessment of nonionic surfactant effect.

It was previously shown that aqueous colloidal solution of C₆₀ obtained by solvent exchange activated reparative processes in cold wound of the skin, increased the proliferative activity of the epidermal cells and thickness of the epithelial layer by 2–3 times.²⁴ In our study, we evaluated regenerative activity of the AFD using the animal wound model.

In particular, we assessed the influence of the AFD on expression of growth factors, cytokines and other parameters involved in the healing process, as well as the cell proliferation activity and histological assay. We have shown previously that the aqueous fullerene C₆₀ dispersion produced by the biocompatible dialysis method possesses the anti-inflammatory effects in a mice model of atopic dermatitis and restores the function of the skin barrier by increasing the filaggrin/mRNA expression, suggesting its action on a redox homeostasis¹¹ or/and with activation of aryl hydrocarbon receptor restoring the filaggrin expression.^{25,26}

Results and discussion

AFD structural characterization

To increase stability of the C₆₀ nanoparticles in the AFD the biocompatible nonionic surfactant was introduced at a low concentration. Our experiments demonstrated that the most effective surfactant was a poloxamer P407/Pluronic® F-127 (molecular mass 12,600).²⁷ Usage of the F-127 to enhance the colloidal stability of the C₆₀ dispersion in saline solution has been previously described and controlled ultrasonication of the fullerene powder in the aqueous solution of the F-127 was used.²⁸ However, currently it was reported that poloxamers can be degraded during sonication involving reactive oxygen species, and the degradation products are toxic for the mammalian cells²⁹ and, therefore, it is not recommended to sonicate the F-127. Nevertheless, the F-127 can be successfully used to produce AFD in combination with TFF without ultrasonication. This method allows obtaining solutions with concentrations of C₆₀ up to 2 g/L if a 0.01 % solution of F-127 is used as a displacing medium instead of pure water.

We characterized the structure of the fullerene C₆₀ aqueous dispersions produced by diafiltration-based technology in order to find the state where fullerene molecules are existed at the

nanoscale, as well as how strongly the addition of the Pluronic F-127 polymeric stabilizer affects to structure of fullerene C₆₀. This information may be obtained primarily through methods of scattering of various radiations with a wavelength comparable to the size of the studied objects such as SANS and SAXS.^{30–33}

Fig. 1 shows comparison of the SANS and SAXS curves for the C₆₀ and C₆₀ + Pluronic AFDs. On a double logarithmic scale, power-law intervals are observed, *i.e.*, scattering data indicate two-level aggregation. This type of scattering can be described using the unified exponential/power-law approximation.³⁴ Main fitting parameters are given in Table 1. As revealed by the parameters of the power-law scattering with an exponent of -4 C₆₀ molecules are assembled in the close-packed primary aggregates with a smooth surface. At the same time, the smoothed nature of the curve (the absence of pronounced diffraction minima/maxima) indicates a significant polydispersity. The size distribution of primary aggregates can be calculated within the framework of the PDI index formalism³⁵ (see inset in Fig. 1). The data of analyzing the ratio of the mean-square deviation to the average radius point out that the primary aggregates in the case of Pluronic presence are slightly larger (an increase is about 15 %) as well as their polydispersity: 40 % *versus* 35 % for a system without Pluronic. This may be indirect evidence demonstrating the coating of fullerenes with a polymer surfactant. However, the characteristic peaks on the UV absorption spectra of C₆₀ molecules in water do not change their positions (Fig. 2), suggesting absence of charge transfer complex formation between Pluronic and the detected primary fullerene aggregates approximately 6-nm of size.

Complete shape overlap of the small-angle scattering curves of neutrons and X-rays in the entire q -range suggests that the aggregates, but not separate fullerene molecules are coated with a polymer stabilizer. This is due to close density of water and surfactant for both X-rays and neutrons; therefore, the contrast of

Table 1

Parameters of unified model fitted to the SANS/SAXS experimental data for water-based fullerene systems.

System	Secondary aggregates' size, R_g , nm	Fractal dimension, D	Primary aggregates	
			Size, $\langle R \rangle$, nm	Dispersion, σ , nm
C ₆₀	25.2	2.9	2.85	1.01
C ₆₀ + PluF127	–	2.15	3.27	1.3

the scattering pattern is ensured only by the presence of fullerene aggregates, like in dispersion without Pluronic. To clarify this issue in detail, further research is needed using the neutron contrast variation technique based on hydrogen/deuterium isotopic substitution.³⁶ However, the detected aggregates seem to be close to those previously observed in aqueous dispersions of C₆₀ with Pluronic obtained by other methods.²⁸

Next, the presence of secondary, less compact aggregation was observed. The power-law exponent modulus < 3 indicates that the AFD systems are fractal cluster with a mass fractal dimension equal to the mentioned exponent. So, in contrast to close-packed formations on a scale of < 10 nm, the secondary aggregates are branched. Their gyration radius is about 25 nm for the aqueous dispersion of fullerene, and it is undetected in SANS/SAXS for the F-127-containing system, therefore, it is exceeded 55 nm achievable in the experimental setups used. This is in accordance with the DLS data determined the hydrodynamic radii of the secondary aggregates as 74 and 32 nm for systems with and without Pluronic, respectively (Fig. 3). At the same time, free primary aggregates are not observed. The clusters of C₆₀ with hydrodynamic radius up to 100 nm and with negative ζ -potential were detected in DLS experiments and scanning electron microscopy (SEM). SEM images of dried

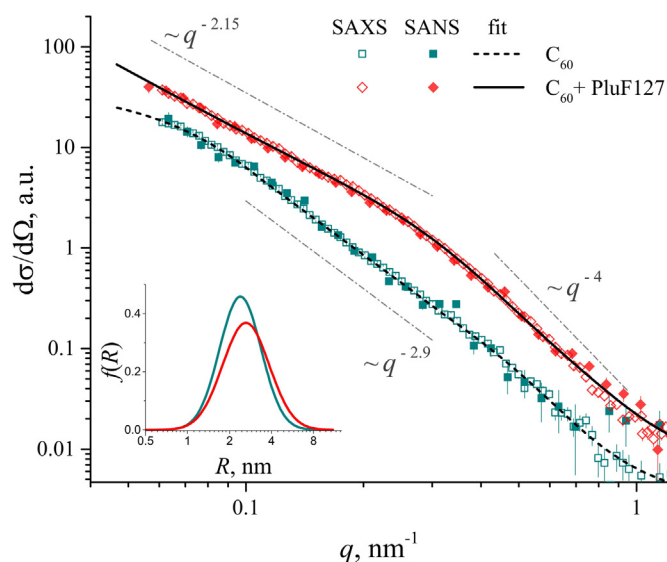


Fig. 1. Comparison of experimental SAXS and SANS curves (points) from initial fullerene dispersion with Pluronic-modified system. Lines denote best models of unified scattering function. Corresponding parameters are given in Table 1. Region corresponding to mass fractal scattering is denoted as well as region of surface scattering. The inset shows the experimentally found radius distribution functions for initial aggregates according to PDI formalism in the lognormal approach.

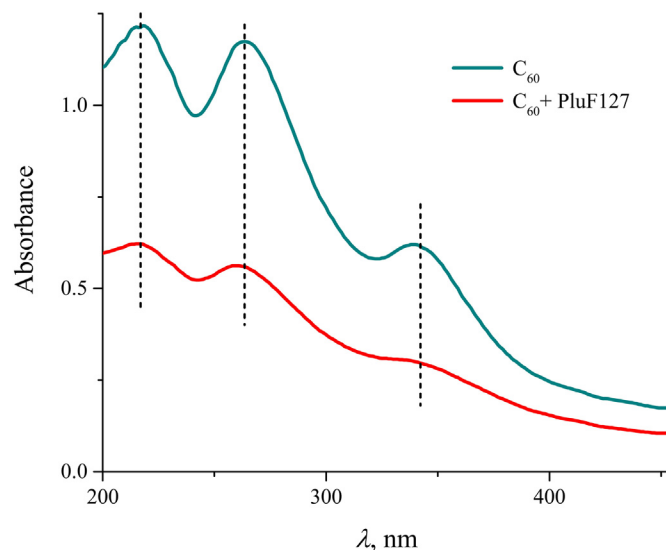


Fig. 2. UV-Vis absorption spectra of C_{60} aqueous dispersion with and without polymeric surfactant. The lines indicate the characteristic absorption peaks of fullerene C_{60} in water.

AFD demonstrated that approximately 100 nm agglomerates consist of smaller subunits.²³ This is in accordance with SANS and SAXS data, which indicate a two-level C_{60} aggregation with different compactness at distinct levels.³³ To be noted the differences in the fractal organization of the two studied dispersions. The C_{60} aqueous dispersion has a fractal dimension of 2.9, which is quite close to that for three-dimensional bodies, while the presence of the Pluronic in the AFD leads to decrease in fractal dimension up to 2.15. These fractal clusters are branched and looser. Thus, despite increase in the average size of aggregates coated with a polymer surfactant, their surface area accessible to the solvent increases significantly, which in turn may have a positive effect on biological activity described further.

AFD regenerative effects in the mouse model of wound healing

Surgical wound and chemical burn models were used to analyze the regenerative activity of the AFD/Pluronic-based ointment in comparison with commercial pharmaceuticals. A visual assessment of the wound healing process was carried out for every mouse by measuring square of the lesion area. The initial average area of damage was $143.5 \pm 6.1 \text{ mm}^2$ (group “before treatment”). On the last day of the experiment, the lesion area for the group was: “without treatment” (self-healing) - $44.4 \pm 6.5 \text{ mm}^2$, “AFD ointment” - $14.8 \pm 2.7 \text{ mm}^2$, “Bepanthen plus” - $26.0 \pm 2.6 \text{ mm}^2$. Fig. 4A, B show photos of the back area of mice after wound damage and treatment. These figures demonstrated

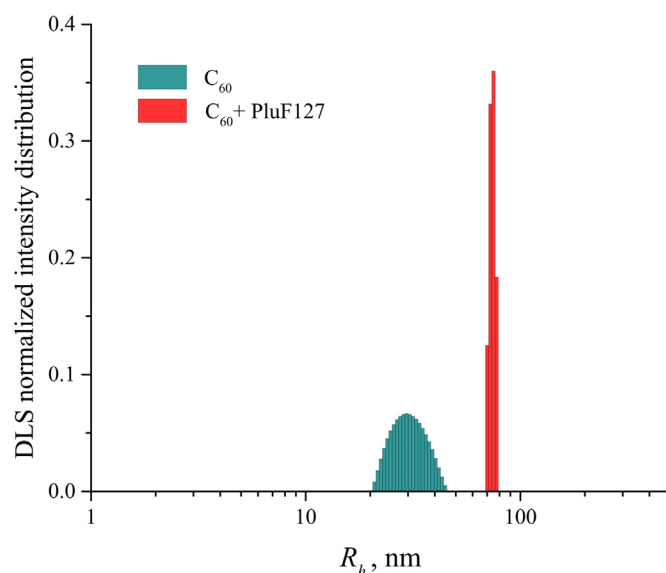


Fig. 3. Distribution of the scattered light intensity according to the hydrodynamic radii of aggregates of the C_{60} fullerene and C_{60} fullerene with Pluronic F-127.

that the healing with AFD ointment in both versions of wounds was effective, the narrowing of the wound area under its action almost the same as in groups treated with commercial Bepanthen plus or Dexpanthenol (D-Panthenol). Since the visual assessment of healing is a subjective parameter, the statistical analysis of wound area between the groups was performed. It was found that if AFD ointment was used to treat the surgical wound (Fig. 4C), its residual area was the smallest. In the case of a burn wound, the effect of AFD ointment was statistically comparable with Dexpanthenol treated group (Fig. 4D). Histological data demonstrated (Fig. 5) that Dexpanthenol reveal the best results in the

treatment of burns, while AFD ointment was slightly inferior in its effectiveness in this case, but its effect was noticeably higher compared to spontaneous healing.

It should be emphasized that active substance of used commercial medicines is Dexpanthenol (R-2,4-dihydroxy-N-(3-hydroxypropyl)-3,3-dimethylbutanamide), a derivative of pantothenic acid (vitamin B5). Dexpanthenol transforms into pantothenic acid which is needed for the synthesis of coenzyme A involved in normal cellular, carbohydrate and fat metabolism. It stimulates skin regeneration, accelerates mitosis, increases the strength of collagen fibers, and exhibit anti-inflammatory

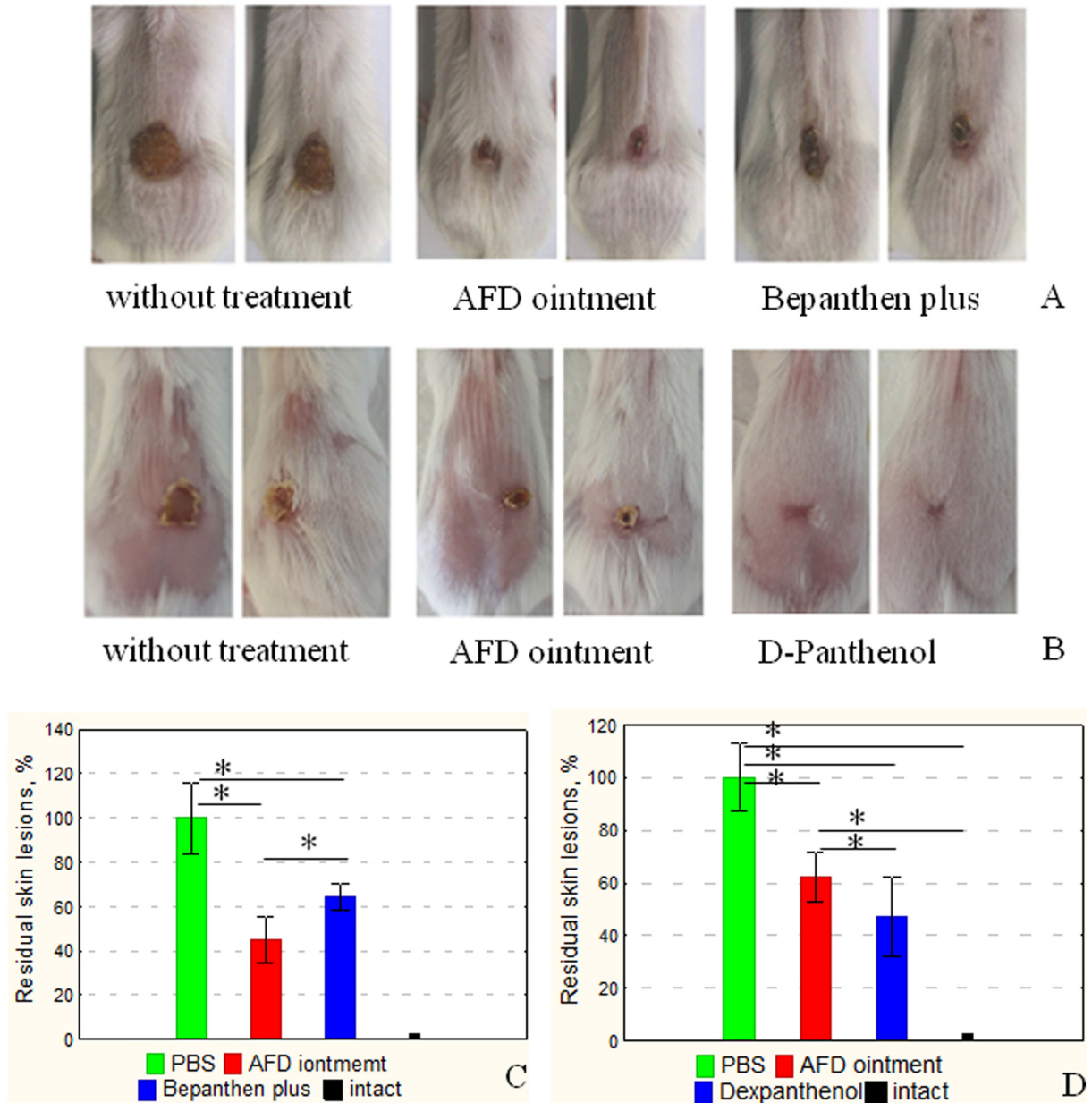


Fig. 4. Wound healing efficiency assessed on day 12. Pictures of the surgical (A) and chemical (B) injuries with treatment AFD or commercial drugs on day 12 and without treatment. Residual skin lesions (%) on day 12 after surgical (C) and chemical (D) wound: “PBS” (mice treated with PBS-containing ointment); “AFD ointment” (mice treated with AFD-containing ointment); “Bepanthen plus” or “D-Panthenol” (mice treated with Bepanthen plus or Dexapanthenol, respectively); “Intact” (untreated animals). Mean ± SE, n = 8, *p < 0.05.

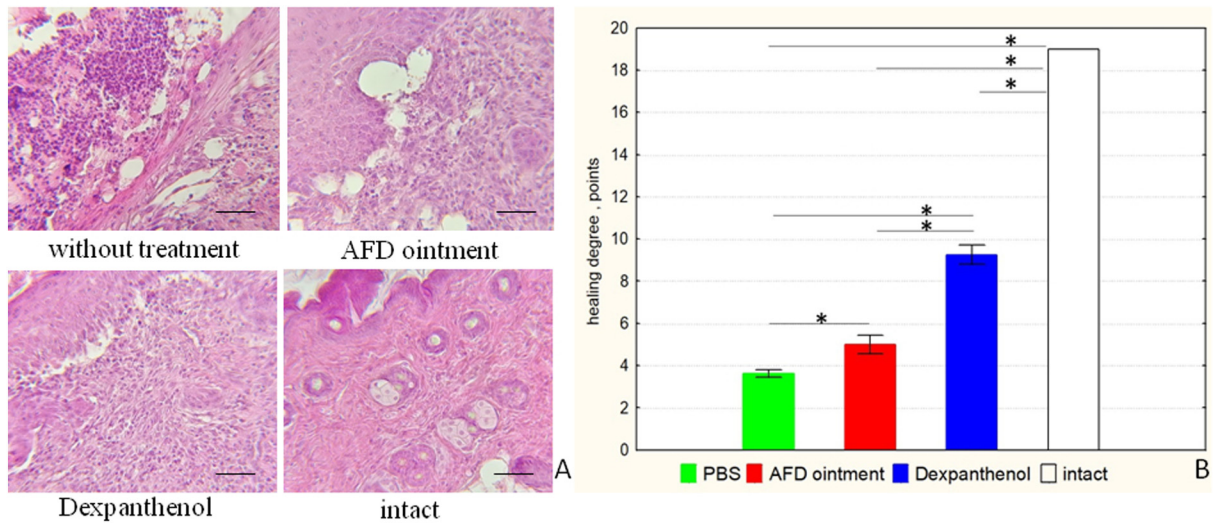


Fig. 5. Histologic features (scale bar 400 μm) (A) and scores obtained for histological analysis of pathologic alterations in mouse skin (B) (mean ± SE, $n = 8$ for each, * $p < 0.05$).

effects.³⁷ However, despite similar therapeutic effects, the mechanisms of action of the Dexpanthenol and fullerene more likely will be different due to a completely unique chemical structure.

In most cases of wound bleeding from damaged vessels and release of the inflammatory mediators, such as serotonin, histamine, vasoactive substances and cytokines into the surrounding tissues are observed. Normal healing involves following phases: inflammation, proliferation, maturation and remodeling. In order to evaluate underlying mechanism of fullerene/AFD healing action, we evaluated gene expression by qPCR of several markers involved in cutaneous wound healing. Firstly, we assessed level of the transcription factor HMGB1 (high-mobility group protein B1) promoted the migration and proliferation of regenerative cells towards inflammation and injury sites³⁸ reduced the risk of scar tissue formation, as well as decreased synthesis of collagen.^{39,40} According to Li W. et al. at the early stage of inflammation the cytosolic HMGB1 attenuated inflammation response by facilitating cell autophagy and preventing cell apoptosis, while at the late stage the extracellular HMGB1 stimulated inflammatory reactions.⁴¹

Analysis of the *hmgbl* expression in the four mouse groups (chemical burn model) demonstrated significant increase of *hmgbl* expression in mice treated with AFD ointment (Fig. 6A). This suggests that the intensification of the regenerative process under the influence of fullerene is observed. The formation of scar tissue during wound healing often correlates inversely with an increase in the overall level of VEGF (vascular endothelial growth factor) involved in angiogenesis.⁴² In addition, *vegf* expression by myeloid cells is a crucial aspect of tissue restoration.⁴³ In a chemical burn model, we found significant increase of *vegf-a* expression in the skin of mice after treatment with AFD ointment (Fig. 6B).

As the anti-inflammatory activity of fullerene was previously shown¹¹ the ability of AFD to suppress the production of pro-inflammatory cytokines TNFα, IL-6 and IL-1α on models of surgical and chemical damages was evaluated. Increases in ex-

pression of these cytokines are observed during the inflammatory phase of healing; in addition, TNFα stimulates production of IL-1, IL-6, and other pro-inflammatory cytokines.^{44,45}

The level of cytokines assessed by qPCR in the skin of mice with surgical and burn wounds after treatment with AFD are shown on Fig. 6. In all experimental groups with surgical wound the level of *tnfα* expression was significantly reduced compared to the “PBS” group (Fig. 6C); the level of *tnfα* in mice with modeled chemical burns was significantly suppressed and similar level in Dexpanthenol-treated animals (Fig. 6D). Gene expression of the pro-inflammatory cytokine *il-6* is significantly increased in wounded skin of both surgical and burn models (PBS columns) compared to intact mice (Fig. 6E, F). IL-6 is one of the most important mediators of the acute phase of inflammation. In IL-6-deficient mice a delay in re-epithelialization of the wound was observed. However, excessive level of IL-6 may provide signals to suppress fibroblast proliferation in the later phase of wound and result to scarring.^{43,46} Probably the suppression of *il-6* production is indicative the anti-inflammatory effect of fullerene C60, which was comparable to Bepanthen plus and Dexpanthenol.

It was previously shown that IL-1α stimulates collagenase production and its overexpression may be mechanistically linked to impaired wound healing through cleavage of collagen.⁴⁷ Moderate increase in *il-1a* gene expression subsequently mediates keratinocyte proliferation at the wound site.⁴⁸ *Il-1a* levels are low in wound fluids from acute wounds, but are elevated in fluids from chronic wounds. Therefore we analyzed mRNA expression of *il-1a* in our experiment. It was found that the *il-1a* gene expression significantly decreased after AFD and Bepanthen plus treatment compare to untreated mice (PBS group). The trend decreased *il-1a* level was observed in “C60” group on model of chemical burn (data not shown). Thus, our results indicate the ability of fullerene C60 to exhibit the anti-inflammatory effect.

The generation of reactive oxygen species including nitric oxide (NO) has a pivotal role in both acute and chronic

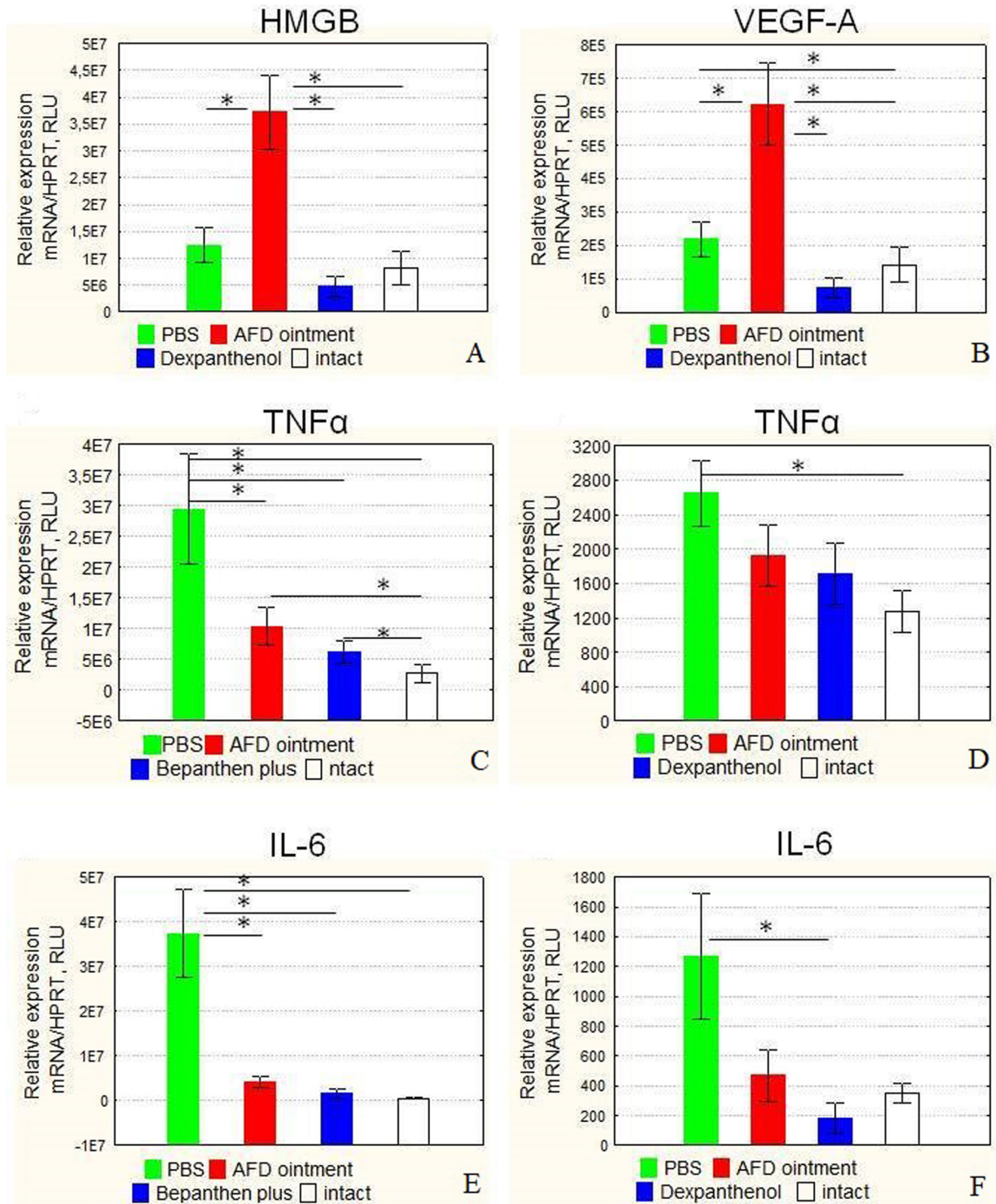


Fig. 6. qRT-PCR analysis of skin tissue of mice with surgical (C, E) and chemical (A, B, D, F) wound: mRNA expression of *hmgbl* (A); *vegfa* (B); *tnfa* (C, D); *il-6* (E, F) (mean ± SE, n = 8 for each, *p < 0.05).

inflammation. The transcription factor Nrf2 is a major regulator of the antioxidant response and is a primary cellular defense mechanism. The Nrf2 neutralize reactive oxygen species and negatively regulate the NF-κB and TGFβ1 signaling pathways. Nrf2(-/-) mice have higher expression of transforming growth

factor β1 (*tgfb1*), the nuclear factor-kappa B (*nf-κb*), fibronectin, and inducible nitric oxide synthase (*inos*).⁴⁹

It was previously shown that the expression of *nrf2* *in vitro* (in melanoma cells) increased after adding the AFD. In addition, on the model of atopic dermatitis we established that fullerene

C60 promoted increasing of filaggrin (*flg*) expression.¹¹ We suppose that the increase of *nrf2* expression can occur as a result of the interaction of fullerene C60 with the aryl hydrocarbon receptor (AhR), which is potent upregulator of *flg*, loricrin (*lor*), and involucrin (*ivl*) expression.⁵⁰ Nrf2 upregulation may result in activation of the Nrf2/HO-1 signaling pathway increasing the antioxidative capacity of cells. Activation of this signaling pathway ultimately leads to suppression of inflammation and contributes to the enhancement of regeneration.⁵¹

Li et al. found that fullerene adduct (carboxyl-Gd3N@C80) efficiently attenuated lipopolysaccharide (LPS) induced oxidative stress in macrophages and suppressed LPS-elicited mRNA expression of pro-inflammatory inducible nitric oxide synthase and tumor necrosis factor-alpha; upregulated antioxidant enzyme axis Nrf2 and heme oxygenase-1, possibly *via* ERK (mitogen-activated protein kinase), but not AKT signaling pathways.⁵² Probably fullerene C60 can interact with macrophages and prevent oxidative stress. We suggest that fullerene C60 interaction with macrophages may result to shift of differentiation to the M2-like phenotype of macrophages which to involved in suppressing of inflammation result in reduced expression of *il-6*, *il-1β* *ι* *tnf-α* and increased production of FGF, EGF, VEGF-A in injured skin.

It is known, that macrophages have a critical role in regeneration processes. The critical value of the macrophage arrival rate in the wound for the process of the limb regeneration was shown on the model of regeneration in the axolotl foot.⁵³ Earlier we have been shown that the AFD addition into a macrophage cell culture increased the expression of CCL2/MCP-1 (Monocyte Chemoattractant Protein 1) in experiments *in vitro* (unpublished data). CCL2/MCP-1 is a powerful chemotaxis factor for monocyte/macrophage in mammals. Thus, in our opinion, the wound healing AFD effect and the low risk of scar formation demonstrated in this work can be associated with fullerene C60 stimulation of the macrophage migration to the inflammation site.

Wound inflammation is often associated with the development of the bacterial infection; so, we assessed the AFD antimicrobial activity. *E. coli* (DH5-Alpha cells) was chosen as a model microorganism for assessing the antibacterial activity of

AFD. This strain of *E. coli* is not a pathogen and non-resistant to antibiotics. Antimicrobial activity of AFD was studied by two methods: 1) disk diffusion test; 2) serial dilution method. In disk diffusion test the inhibition zone where the bacteria have not grown enough to be visible was determined. In serial dilution method the minimum inhibitory and bactericidal concentrations were determined. As a result, it was shown that AFD did not inhibit bacterial growth and did not have bactericidal activity (data not shown). In our opinion, the wound healing AFD effect is associated with its anti-inflammatory activity, as previously established.¹¹

AFD biocompatibility

Experiments *in vivo* and *in vitro* were carried out to study of the AFD biocompatibility. The results of the *in vitro* experiments shown lack of cytotoxicity of AFD in A549, HepG2 and HeLa cell lines. Thus, for concentration range 500–0,08 mg/L the toxicity of the C60 aqueous dispersion was at the same level with the negative control measurements (DMEM without AFD), confirming high biocompatibility.³³ The AFD hemolytic activity was studied using concentrations of C60: 100; 50; 25; 12.5; 6.25; 3.12 μg/mL. According to the concentrations of C60 used the degree of hemolysis was: 25, 14, 7, 4, 2 and 0.5 %, respectively. Thus, the C60 has a low level of hemolytic activity.

Skin toxicity experiments were performed to test the AFD biocompatibility. Rats were treated with AFD subcutaneously to the withers or intramuscularly in the thigh area in dose of 2 mg once. The negative control group was treated with water for injection. Visual inspection of the injection site was performed daily. Skin lesions for histological analysis were taken on the 7th day after the injection. It was shown that there were no pathological changes in the rat skin after the AFD injection (Fig. 7).

There were no differences between the experimental and control (intact) mice in the appearance, motor activity and behavioral reactions: mobility was normal, the forced posture was absence, the coat was clean, the vibrissae were preserved. Maintaining an adequate response to external stimuli, active behavior, and frequent grooming were noted. There were no

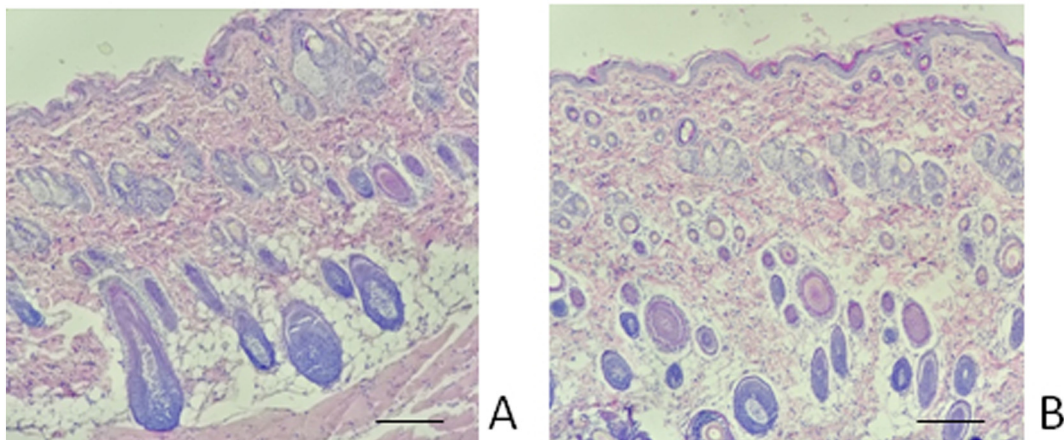


Fig. 7. AFD skin toxicity. Histologic features (scale bar 100 μm). Rats were treated with AFD subcutaneously to the withers in dose of 2 mg once (A). The negative control group was treated with water for injection (B).

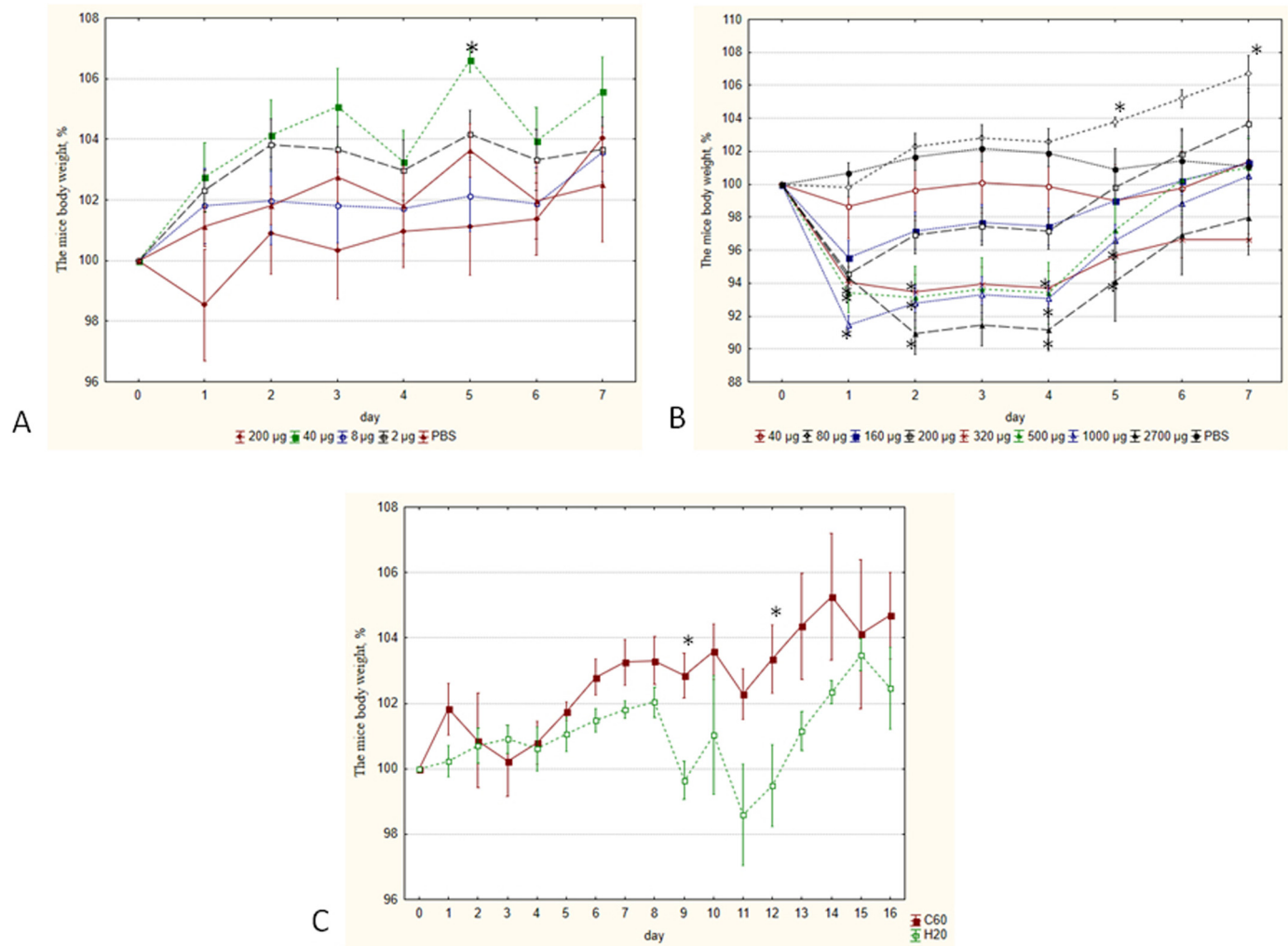


Fig. 8. The dynamic of changes in the mice body weight using different doses of AFD. AFD doses (i.v. injection) (A): 200 µg of C60 (“200 µg”); 40 µg of C60 (“40 µg”); 8 µg of C60 (“8 µg”); 2 µg of C60 (“2 µg”); 0 µg of C60 (“PBS”); AFD doses (i.p. injection) (B): 40 µg of C60 (“40 µg”); 80 µg of C60 (“80 µg”); 160 µg of C60 (“160 µg”); 200 µg of C60 (“200 µg”); 320 µg of C60 (“320 µg”); 500 µg of C60 (“500 µg”); 1000 µg of C60 (“1000 µg”); 2700 µg of C60 (“2700 µg”); 0 µg of C60 (“PBS”); (C) AFD doses (i.g. administration): 1000 µg of C60 (“C60”); water for injection (“H2O”). * - p < 0,05.

involuntary and abnormal movements: convulsions, tremor, myoclonus, playpen movements, tic forms, as well as paralysis and paresis; there were no signs of neurological disorders of the pyramidal, extrapyramidal pathways, as well as bulbar symptoms. The mice had completely preserved coordination capabilities and physiological reflexes. Urination and defecation were free. The color and smell of feces and urine were specific. The feces were moderately soft, formed. The abdomen was soft and painless, visible mucous membranes were pink and moist. The skin was not damaged, the claws were preserved. Pathological changes of pads were absence. The perianal, perioral and peri-orbital areas were clean; the external auditory meatus was free, clean and dry. There was no death of mice after a single intravenous AFD injection in various doses.

No significant body weight loss was observed in mice after AFD injection (intravenously) (Fig. 8A), however, some tendency to weight loss (1.5 % or 0.3 g) was observed after injection in dose of 200 μg . In the control group of mice, the same fluctuation of body weight was noted on 4–6 days of the observation. It should be noted that administration of AFD at doses of 2 and 40 μg resulted in an increase in body weight in mice. All this suggests that the AFD administration did not lead to toxic manifestations and changes in the behavior of animals.

Further, the toxic effect of fullerene C60 was studied after single intraperitoneal (i.p.) AFD injection in various doses. The change in body weight of animals is shown in Fig. 8B.

It was shown that a single i.p. injection of C60 fullerene did not lead to the animal death and did not affect on the mouse behavioral during 7 days of the observation. The Fig. 8B shows that the introduction of AFD in high doses of C60 (500, 1000 and 2700 μg) lead to a significant decrease of the animal body weight. It is important that the difference in the weight of the experimental and control animals became the same on the 6th

day of observation. The weight difference of animals treated with 500 μg of C60 and PBS was not detected on the 7th day of monitoring. There was no found any significant difference between group of mice treated with the AFD in C60 doses up to 500 μg and control animals. However, the significant increase of weight of animals was observed on the 5th day after AFD injection (in C60 dose 80 μg).

The toxic effect of fullerene C60 was studied after single intragastric (i.g.) AFD administration (in C60 dose 1000 μg). The change in body weight of animals is shown in Fig. 8C.

The average mice body weight did not statistically differ in the experimental and the control groups. It should be noted that the weight gain AFD was better in mice received than in the control group (especially on the 9th and 12th days of observation). The death of animals after a single injection of AFD was not observed. Behavioral reactions of the control and experimental groups of mice did not differ, as well as pathological changes during clinical examination. Thus, these data provide evidence that AFD are not toxic by these routes of administration.

The histological analysis was shown the absence pathological signs of inflammation, necrosis, hemorrhage, edema in the internal organs (Fig. 9).

In the experimental and the control groups the internal cavities of the body did not contain free or encysted fluid. The irritating effect of AED and the solvent on the mucous membrane of the gastrointestinal tract was not revealed. The digestive glands were also studied and external pathological changes were not found in the liver and pancreas. Histological characteristics of kidneys, the uterus and ovaries were normal. Pathological changes indicating inflammatory, necrotic, hypoplastic or hyperplastic processes, dystrophy and atrophy, hemorrhages and neoplasms in the above organs and tissues of mice, both in the

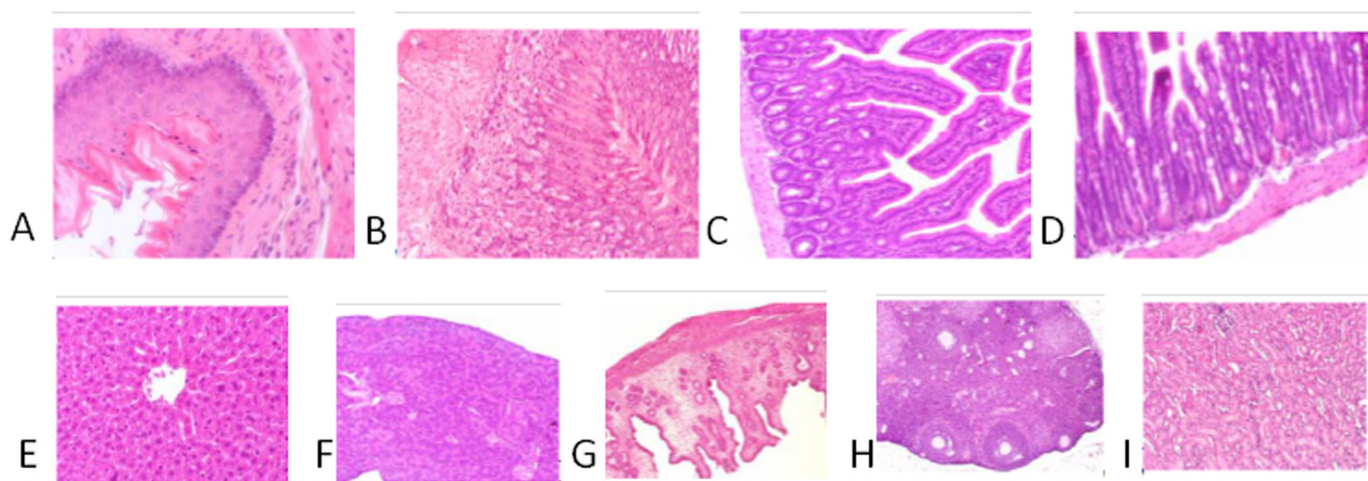


Fig. 9. Histological analysis of the gastrointestinal tract, the liver, kidneys, pancreas, uterus and ovaries. A. Mouse esophagus after intragastric administration of fullerene suspension, stained with hematoxylin-eosin, magnification 400. B. Mouse stomach after intragastric administration of fullerene suspension, stained with hematoxylin-eosin, magnification 400. C. Mouse jejunum after intragastric administration of fullerene suspension, stained with hematoxylin-eosin, magnification 200. D. Mouse colon after intragastric administration of fullerene suspension, hematoxylin-eosin staining, magnification 200. E. Mouse liver after intragastric administration of fullerene suspension, stained with hematoxylin-eosin, magnification 400. F. Mouse pancreas after intragastric displacement of fullerene suspension, stained with hematoxylin-eosin, magnification 200. G. Mouse uterus after intragastric administration of fullerene suspension, stained with hematoxylin-eosin, magnification 100. H. Mouse ovary after intragastric injection of fullerene suspension, hematoxylin-eosin stain, magnification 100. I. Mouse kidney after intragastric injection of fullerene suspension, hematoxylin-eosin stain, magnification 200.

experimental and control groups were not detected. Thus, macroscopic and microscopic examination of the internal organs and tissues of experimental mice showed the absence of toxic and irritating effects of AFD.

Conclusion

Analysis of the aqueous dispersions of C₆₀ fullerene with Pluronic F-127 revealed that the tangential flow filtration process of aggregation is carried out *via* complex two-step mechanism. C₆₀ fullerene molecules initially forms dense aggregates several nanometers in size and then they are associated in secondary fractal aggregates partially covered with nonionic polymeric surfactant. The later have branched structure with developed surface area and exhibit biological activity.

We have shown that AFD has practically no hemolytic activity and a toxic effect regardless of the route of administration. At the same time, a noticeable increase in body weight was observed in AFD groups with small doses. Histological analysis also did not reveal pathological changes in the internal organs characteristic of toxic damage.

Visual monitoring of the healing process and histological analysis of the skin biopsy demonstrated that effectiveness of the AFD ointment is comparable to commercial healing drugs Bepanthen plus and Dexapanthenol. Anti-inflammatory effect of AFD was confirmed by significant suppression of the pro-inflammatory cytokines *tnf α* , *il-6* and *il-1 α* expression. This effect was more pronounced on model of surgical wound. We suppose that risk of scarring was reduced in AFD treated mice since the *hmgbl* expression level was increased. Elevated level of *vegfa* expression associated with AFD-therapy indicates activation of angiogenesis and development of fibrous type of wound healing.

The AFD ointment is a potential therapeutic tool for therapy of the skin defects caused by both acute and chronic wounds. Elevated *hmgbl* and *vegfa* expression level stimulated by AFD ointment can be used in regenerative medicine to prevent the formation of scar tissue during wound healing. Our study has shown that AFD ointment is useful as add-on therapy to existing healing remedies by reducing the risk of scarring.

We also believe that Pluronic unaffected the anti-inflammatory properties of the C₆₀ diafiltration dispersion, since our previous study of C₆₀ dispersion without Pluronic on a model of atopic dermatitis also showed a significant anti-inflammatory action.¹¹ We suggest that in the skin fullerene interacts with the aryl hydrocarbon receptor, stimulates expression of *nrf2* resulting in activation of the Nrf2/HO-1 signaling pathway that in turn increase the antioxidant capacity of cells. In addition, the fullerene C₆₀ anti-inflammatory and regenerative activity may be defined by macrophage activation.

The structure of fullerene clusters affects their biological activity. In this study we characterize 3D structure of the fullerene C₆₀ aqueous dispersion using the small-angle neutron scattering method in detail and observed pronounced regenerative activity of AFD. Taken together these results indicate that aqueous dispersion of the fullerene C₆₀ would have great potential in the therapy of surgical and chemical wound.

Experimental

Materials

AFD preparation

1000 mg of pristine fullerene C₆₀ powder (NeoTec product, Russia 99.95 %) was dissolved (~3 h) in 1600 mL of *N*-methyl-1-pyrrolidone (NMP, Sigma-Aldrich, 99.5 %) and obtained purple solution was then passed through glass fiber filter (Sigma-Aldrich, 2.6 mm) and 1600 mL of deionized water was added to the filtrate. Obtained mixture was subjected to TFF using peristaltic pump (Spectrumlabs Krosflo ACR1-U20-01N) and Pellicon 2 Ultracel 100 kDa membrane (regenerated cellulose) ultrafiltration cassette module and stainless steel holder (Millipor/Merck); 0.01 % solution of Pluronic F-127 was used as a replacement medium. The process of removing NMP from C₆₀-containing retentate was monitored by the quantification of NMP by spectrophotometry in permeate and was finalized after the practical disappearance of band at 190–210 nm which characteristic for free NMP absorption. Ultrafiltration was continued without supplying a replacement solution in order to concentrate the resulting C₆₀ dispersion (retentate) to an approximate content of 1 g/L. The yield of the final brownish clear solution, AFD, was ~900 mL (stored at 10 °C protected from light). Elemental analysis of vacuum-dried sample (%): C 78.62, H 1.11, N 2.28. The C₆₀ content was quantified by spectrophotometry (Cary 100, Agilent Technologies, 10 mm cell) using a calibration curve of its molar extinction coefficient at 340 nm ($\epsilon = 50,200$) measured before.²¹

AFD ointment

For the experimental treatment of wound damage, an AFD-containing ointment (composition: AFD:vaseline:sucrose palmitate = 40:36:24 (by weight)) was made using the IKA 25 digital ultra-turrax as a mixing device; designation as “AFD ointment”.

Structural methods

Small-angle neutron scattering

First, radiation scattering methods were used to analyze the structure at the nanoscale. Thus, SANS is able to provide information on nanoobjects in bulk samples without special preparation due to the high penetrating power of neutrons and sensitivity to light isotopes. SANS measurements were carried out at the YuMO small-angle time-of-flight diffractometer with double-detector system.⁵⁴ YuMO is located on the 4th channel of IBR-2 pulsed neutron source (FLNP JINR, Dubna, Russia). The neutron wavelengths, λ , within a range of 0.05–0.8 nm, the sample-detector distances of 4.5 and 13 m and calibration vanadium standard were used to obtain differential cross-section per sample volume, $d\sigma/d\Omega(q)$, as a function of the module of momentum transfer, q , in the range of 0.06–2 nm⁻¹. All SANS measurements were made in Hellma plane quartz cells (path length 1 mm). The raw data treatment was performed by the SAS program with a smoothing mode.⁵⁵

Small-angle X-ray scattering

Complementary SAXS measurements were carried out on a Rigaku S-MAX 3000 experimental facility with a Cu rotating

anode (MIPT, Dolgoprudniy, Russia) using a standard transmission configuration. SAXS spectra were obtained in a q -range of $0.06\text{--}2\text{ nm}^{-1}$ operating at the X-ray wavelength of 0.154 nm . The samples studied were placed in borosilicon capillaries having 1.5 mm diameter and 0.01 mm wall thickness (W. Muller, Berlin, Germany).

UV-Vis absorption

UV-Vis absorption spectra as a dependence of optical density on wavelength were recorded using the spectrophotometer NanoPhotometer P360 (Implen GmbH, Germany) in a range of $200\text{--}650\text{ nm}$ at room temperature. The AFDs were placed in polymethylacrylate cells having an optical path length of 1 cm .

Dynamic light scattering

The size distributions of fullerene aggregates were estimated DLS (also known as photon correlation spectroscopy or quasi-elastic light scattering). Photocor Compact-Z instrument equipped with a TEC stabilized diode laser (max. power 25 mW , wavelength 638 nm) was used.

Biological experiments

The surgical wounds and chemical burns animal models

Female 4- to 6-week-old BALB/c mice (Stolbovaya, Moscow, Russia) were kept under pathogen-free conditions. Experiments with animals were carried out in accordance with the EU Directive 2010/63/EU for animal experiments. All experimental protocols were reviewed and approved by the local ethical committee of NRC Institute of Immunology FMBA of Russia.

Animals were anesthetized using 4% isoflurane for 2 min via the respiratory route, Lidocaine 0.5% was injected locally before surgical incision and alkali burn of the skin. To inflict a surgical wound a piece of skin ($1 \times 1\text{ cm}$) from the back of mice BALB/c was excised. To induce alkali burn inflammation a solution of 12.5 N NaOH (Merck, Germany) on cotton pads ($1 \times 1\text{ cm}$) was applied to the shaved back area for 60 s . The AFD ointment was applied to the wound surface ($40\text{ }\mu\text{g C}_{60}$ /mouse) in 24 h after surgery (group "AFD ointment"). As a control widely used therapeutics Bayer Bepanthen Plus cream and Dexpanthenol ointment were used to treat surgical wounds (Bepanthen plus group) and alkali burn (Dexpanthenol), respectively. The ointment contained PBS instead of AFD was used as negative control ("PBS" group). The "Intact" group (without any skin damage) was used as negative control too. The listed formulations were applied once per day for 11 days . On day 12 mice were sacrificed and skin samples were collected for qPCR analysis and histologic examination.

Evaluation of wound healing effectiveness

The skin healing rate was evaluated by measuring the area of the wound in the longitudinal and transverse directions (mm) daily. Then, the wound area was calculated by the formula:

$$S_{el} = \pi ab \quad (1)$$

where S_{el} - the area of the ellipse, a - the semi-major axis (half of the long diameter or transverse dimension), b - the semi-axis (half of the short diameter or longitudinal dimension).

Wound healing efficiency (X) was calculated as a percentage according to the formula:

$$X = (1 - S_k/S_1) \times 100\% \quad (2)$$

where S_k - the final wound area, S_1 - the initial wound area.⁵⁶

Real-time PCR

The total RNA from skin samples was extracted using the RNeasy Mini Kit (Qiagen, Courtaboeuf, France) according to the manufacturer's instructions. cDNA was synthesized using "Reverta-L kit" (Interlabservice, Russia). The reverse transcription reaction product was amplified via qRT-PCR using an iCyclerIQ Real-time PCR Detection System (Bio-Rad Laboratories) and PCR Mix kit (Syntol, Russia). Primers and probes used in this study are described in Table 3.

Calculations to determine the relative level of gene expression were made using the comparative Ct method (ΔCt) referring to the mHPRT in each sample; the results are presented as arbitrary units.

Relative quantification of RT-qPCR was used to detect changes in expression of the target genes relative to a reference gene, which is housekeeping mice *hprt*. Quantitative PCR results for mRNA expression are presented as ΔCt values, calculated by the formula: ratio (reference/target) = $2^{\text{Ct}(\text{hprt}) - \text{Ct}(\text{gene of interest})}$.⁵⁷

Histological analysis

The skin specimens from the alkali burned mice, gastrointestinal tract, liver, pancreas, kidneys, uterus, and ovaries were collected, fixed overnight with 10% paraformaldehyde at $4\text{ }^\circ\text{C}$, paraffined and consecutive $4\text{ }\mu\text{m}$ sections were cut for hematoxylin-eosin (H&E) staining using Finesse™ E + Microtome (Finland). Sections stained with H&E were imaged using a light microscope (Leica DM2000, Germany) with $50\times$, $100\times$, and $400\times$ lenses. The histopathological changes in the skin were graded according to a modified semiquantitative scoring system by a blinded investigator (Table 2). Following parameters were

Table 2
Assessment of skin lesions.

Skin layer	Parameter	0 point	1 point	2 points	3 points
Epidermis	Epidermis thickening	Pronounced	Moderate	Mild	Absent
	Stratification of keratinocytes	Absent	Present	–	–
	Necrosis	Present	Absent	–	–
Dermis	Proliferation of connective tissue components	Pronounced	Moderate	Mild	Absent
	Leukocyte infiltration	Pronounced	Moderate	Mild	Absent
	Necrosis	Present	Absent	–	–
Subcutaneous fat	Proliferation of connective tissue components	Pronounced	Moderate	Mild	Absent
	Leukocyte infiltration	Pronounced	Moderate	Mild	Absent
	Necrosis	Present	Absent	–	–

Table 3
Sequences of primers and probes.

Oligonucleotide	Sequences (5'-3')	Target gene
Reverse primer	CTTTAATGTAATCCAGCAGGTCAG	<i>hprt</i>
Forward primer	TATACCTAATCATTATGCCGAGGAT	<i>hprt</i>
Reverse primer	TGAGAAGTTGACAGAAGCATCC	<i>hmgbl</i>
Forward primer	GGCAAAGGAGATCCTAAGAAGC	<i>hmgbl</i>
Reverse primer	GTCGGTCTCACTACCTGTGTATG	<i>il1a</i>
Forward primer	CTCAGATTCACAACCTGTTCTGTG	<i>il1a</i>
Reverse primer	GTTTCTGTATCTCTGAAGGACTC	<i>il6</i>
Forward primer	GCTACCAAAGTGGATATAATCAGG	<i>il6</i>
Reverse primer	CTGGGCCATAGAACTGATGAG	<i>tnfα</i>
Forward primer	GCTCTTCTGTCTACTGAACTTCG	<i>tnfα</i>
Reverse primer	GTGATGTTGCTCTCTGACGTG	<i>vegfa</i>
Forward primer	CTTCAAGCCGCTCTGTGTG	<i>vegfa</i>
HPRT-FAM	FAM-TCCTCATGGACTGATTATGGA-CAGGACT-BHQ1	<i>hprt</i>
HMGB1-FAM	FAM-GCCGGGAGGAGCACAAGAAGAAG-BHQ1	<i>hmgbl</i>
IL1a-FAM	FAM-CGTGTTGCTGAAGGAGTTGCCAGABHQ1	<i>il1a</i>
IL6-FAM	F A M - C T G G T C T T G A G T A C C A - TAGCTACCTGG-RTQ1	<i>il6</i>
TNFα-FAM	FAM-TGAGAAGTTCCCAAATGGCCTCCC-BHQ1	<i>tnfα</i>
VEGF-A-FAM	FAM-CTGTGCAGGCTGCTGTAACGATG-RTQ1	<i>vegfa</i>

evaluated: the thickness of the epidermis, proliferation of connective tissue cells in the dermis and subcutaneous fat (SCF), the presence of necrosis, keratinocyte stratification and leukocyte infiltration. The points for every parameter were summarized.

Experiment protocol for acute toxicity analyzes

The AFD was administered intravenously (i.v.), intraperitoneally (i.p.), and intragastrically (i.g.).

i.v. administration. Mice BALB/c (weight 20 g) were divided into 5 groups. Groups 1, 2, 3, and 4 received AFD based on C60 doses of 2, 8, 40, and 200 µg, respectively. Control group 5 was treated with phosphate-buffered saline (PBS). Animal behavior and their weight were monitored within 7 days after treatment.

i.p. administration. Mice were divided into 9 groups. Groups 1–8 received AFD in C60 doses of 40, 80, 160, 200, 320, 500, 1000 and 2700 µg, respectively. Animals of the 9th group were injected with PBS. The behavior of the animals and their weight were observed for 7 days after treatment with AFD.

i.g. administration. Mice were treated with AFD in C60 dose 1 mg. Animals of the control group received water in the same volume. Mice body weight control and daily clinical examination were carried out for 16 days after administration. The clinical examination procedure included an assessment of the external condition (the condition of the skin, nasal cavity and external auditory canal, the condition of the perianal, perioral and periorbital regions, defecation, urination). The necropsy procedure was carried out on day 16 of experiment. The gastrointes-

tinal tract, liver, pancreas, kidneys, uterus, and ovaries were taken for histological examination.

Statistical analysis

Statistical analysis was performed using Statistica 8.0 (StatSoft Inc., USA) software. Statistical significance was determined by Student's criterion. Data were accepted as significantly different when $P < 0.05$. The data are shown as mean \pm SE.

CRedit authorship contribution statement

All authors contributed to the writing of the manuscript and have approved the final version for publication.

SNN, NAA, KOY and MEA carried out work with animals, performed the real-time PCR analysis, histological analysis and statistical processing. ASM and TEA prepared the AFD and ointment. ASM, SNN, TAA, POA, KMR and AMV made contributions to the concept and wrote the manuscript. KDA, DAS and KMR made contributions in the interpretation of biological experimental data. TAA, IOI, KOA, TOV, AMV provided all instrumental measuring and made substantial contributions in interpretation spectral data.

Declaration of competing interest

The authors declare no commercial or financial conflict of interest.

Acknowledgements

This study was supported by the program of cooperation JINR–Czech Republic No.182/18.03.2021/25 and by a Megagrant of the Government of the Russian Federation, grant number 14.W03.31.0024 (075-15-2021-632).

Funding

This study did not receive any specific grant from funding agencies in the public or nonprofit sector.

References

1. Werner S, Grose R. Regulation of wound healing by growth factors and cytokines. *Physiol Rev* 2003;**83**:835-70 Werner S, Antsiferova M, Smola H. Skin wound healing. In book: Pathobiology of Human Disease, 2014.
2. Checa J, Aran M. Airway redox homeostasis and inflammation gone awry: from molecular pathogenesis to emerging therapeutics in respiratory pathology. *Int J Mol Sci* 2020;**21**:9317.
3. Schafer M, Werner S. Oxidative stress in normal and impaired wound repair. *Pharmacol Res* 2008;**58**:165-71.
4. Noori S. *An Overview of oxidative stress and antioxidant defensive system* 2012;**1**:413.
5. Scar Treatment Market Size, Share & Trends Analysis Report By Scar Type (Atrophic, Hypertrophic & Keloid Scars, Stretch Marks), By Product (Injectables, Topical, Laser), By End Use, And Segment Forecasts, 2019–2026. <https://www.grandviewresearch.com/industry-analysis/scar-treatment-market>.

6. Bosi S, Da Ros T, Spalluto G, Prato M. Fullerene derivatives: an attractive tool for biological applications. *Eur J Med Chem* 2003;**38**:913-23.
7. Roursgaard M, Poulsen SS, Kepley CL, Hammer M, Nielsen GD, Larsen ST. Polyhydroxylated C60 fullerene attenuates neutrophilic lung inflammation in mice. *Basic Clin Pharmacol Toxicol* 2008;**103**(4):386-8.
8. Magoulas GE, Garnelis T, Athanassopoulos CM, Papaioannou D, Mattheolabakis G, Avgoustakis K, et al. Synthesis and antioxidative/anti-inflammatory activity of novel fullerene-polyamine conjugates. *Tetrahedron* 2012;**68**:7041-9.
9. Yudoh K, Karasawa R, Masuko K, Kato T. Water-soluble fullerene (C60) inhibits the development of arthritis in the rat model of arthritis. *Int J Nanomedicine* 2009;**4**:217-25.
10. Kuznietsova H, Dziubenko N, Hurmach V, Chereschuk I, Motuziuk O, Ogloblya O, et al. Water-soluble pristine C60 fullerenes inhibit liver fibrotic alteration and prevent liver cirrhosis in rats. *Oxidat Med Cell Longevity* 2020;8061246.
11. Shershakova N, Baraboshkina E, Andreev S, Purgina D, Struchkova I, Kamyshnikov O, et al. Anti-inflammatory effect of fullerene C60 in a mice model of atopic dermatitis. *J Nanobiotechnol* 2016;**14**:8.
12. Gharbi N, Pressac M, Hadchouel M, Szwarc H, Wilson SR, Moussa F. Fullerene is a powerful antioxidant in vivo with no acute or subacute toxicity. *Nano Lett* 2005;**5**:2578-85.
13. Zhou Z, Joslin S, Dellinger A, Ehrich M, Brooks B, Ren Q, et al. A novel class of compounds with cutaneous wound healing properties. *J Biomed Nanotech* 2010;**6**:605-11.
14. Sinha N, Thakur AK. Regeneration of lung epithelial cells by Fullerene C60 nanoformulation: A possible treatment strategy for acute respiratory distress syndrome (ARDS). *BioRxiv* preprint.
15. Yudoh K. Water-soluble fullerene (C60) inhibits the development of arthritis in the rat model of arthritis. *Int J Nanomedicine* 2009;**4**:217-25.
16. Wakimoto T, Uchida K, Mimura K, Kanagawa T, Mehandjiev TR, Aoshima H, et al. Hydroxylated fullerene: a potential antiinflammatory and antioxidant agent for preventing mouse preterm birth. *Am J Obstet Gynecol* 2015;**213**(5):708.e1-708.e708.
17. Dellinger A, Zhou Z, Lenk R, MacFarland D, Kepley CL. Fullerene nanomaterials inhibit phorbol myristate acetate-induced inflammation. *Exp Dermatol* 2009;**18**:1079-81.
18. Andrievsky GV, Kosevich MV, Vovk OM, Shelkovsky VS, Vashchenko LA. On the production of an aqueous colloidal solution of fullerenes. *J Chem Soc Chem Commun* 1995;**1281-1282**.
19. Deguchi RG, Tsujii Alargova K. Stable dispersions of fullerenes, C60 and C70, in water. Preparation and characterization. *Langmuir* 2001;**17**:6013-7.
20. Mchedlov-Petrosyan NO. Fullerenes in liquid media: an unsettling intrusion into the solution chemistry. *Chem Rev* 2013;**113**(7):5149-93.
21. Andreev S, Purgina D, Bashkatova E, Garshev A, Maerle A, Andreev I, et al. Study of fullerene aqueous dispersion prepared by novel dialysis method: simple way to fullerene aqueous solution. *Fullerenes, Nanotub Carbon Nanostruct* 2015;**23**:792-800.
22. Brumberger H, editor. *Modern Aspects of Small-Angle Scattering*. Dordrecht: Kluwer Academic Publishers; 1995.
23. Klimova R, Andreev S, Momotyuk E, Demidova N, Fedorova N, Chernoryzh Y, et al. Aqueous fullerene C60 solution suppresses herpes simplex virus and cytomegalovirus infections. *Fuller Nanotub Carbon Nanostructures* 2020;**28**:487-99.
24. Vlasov OO, Kovalov GO, Myroshnychenko MS. Morphological assessment of wound healing after cryodestruction of skin using an aqueous colloidal solution of C60 fullerenes. *Wiad Lek* 2020;**73**(4):642-7.
25. Tsuji G, Hashimoto-Hachiyu A, Kiyomatsu-Oda M, Takemura M, Ohno F, Ito T, et al. Aryl hydrocarbon receptor activation restores filaggrin expression via OVOL1 in atopic dermatitis. *Cell Death Dis* 2017;**8**(7)e2931.
26. Tkachev Ya, Shershakova N, Kozhikhova K, Turetskiy E, Andreev S. Comparative modeling of the interaction of C60 fullerene with the human aryl-hydrocarbon receptor. https://istina.msu.ru/download/243128156/1kRT2S:phjIVgC_nLUy9yqvdmbnF18wRY/ (in Russian).
27. Kabanov AV, Lemieux P, Vinogradov S, Alakhov V. Pluronic® block copolymers: novel functional molecules for gene therapy. *Adv Drug Del Rev* 2002;**54**:223-33.
28. Aich N, Boateng LK, Flora JRV, Saleh NB. Preparation of non-aggregating aqueous fullerenes in highly saline solutions with a biocompatible non-ionic polymer. *Nanotechnology* 2013;**24**395602.
29. Banerjee S. Molecular dynamics study of self-agglomeration of charged fullerenes in solvents. *J Chem Phys* 2013;**138**044318.
30. Avdeev MV, Khokhryakov AA, Tropin TV, Andrievsky GV, Klochkov VK, Derevyanchenko LI, et al. Structural features of molecular-colloidal solutions of C60 fullerenes in water by small-angle neutron scattering. *Langmuir* 2004;**20**:4363-8.
31. Kyzyma EA, Tomchuk AA, Bulavin LA, Petrenko VI, Almasy L, Korobov MV, et al. Structure and toxicity of aqueous fullerene C60 solutions. *J Surf Invest* 2015;**9**:1-5.
32. Prylutska S, Panchuk R, Gołuński G, Skivka L, Prylutskiy Yu, Hurmach V, et al. C60 fullerene enhances cisplatin anticancer activity and overcomes tumor cell drug resistance. *Nano Res* 2017;**10**:652-71.
33. Tomchuk AA, Shershakova NN, Andreev SM, Turetskiy EA, Ivankov OI, Kyzyma OA, et al. C60 and C60-arginine aqueous solutions: in vitro toxicity and structural study. *Fuller Nanotub Carbon Nanostructures* 2020;**28**:245-9.
34. Beaucage G. Approximations leading to a unified exponential/power-law approach to small-angle scattering. *J Appl Cryst* 1995;**28**:717-28.
35. Beaucage G, Kammler HK, Pratsinis SE. Particle size distributions from small-angle scattering using global scattering functions. *J Appl Cryst* 2004;**37**:523-35.
36. Avdeev MV. Contrast variation in small-angle scattering experiments on polydisperse and superparamagnetic systems: basic functions approach. *J Appl Cryst* 2007;**40**:56-70.
37. Proksch E, de Bony R, Trapp S, Boudon S. Topical use of dexpanthenol: a 70th anniversary article. *J Dermatolog Treat* 2017;**28**:766-73.
38. Palumbo R, Sampaolesi M, De Marchis F, Tonlorenzi R, Colombetti S, Mondino A, et al. Extracellular HMGB1, a signal of tissue damage, induces mesoangioblast migration and proliferation. *J Cell Biol* 2004;**164**:441-9.
39. Ranzato E, Patrone M, Pedrazzi M, Burlando B. Hmgb1 promotes wound healing of 3T3 mouse fibroblasts via RAGE-dependent ERK1/2 activation. *Cell Biochem Biophys* 2010;**57**:9-17.
40. Zhang Q, O'Hearn S, Kavalukas SL, Barbul A. Role of high mobility group box 1 (HMGB1) in wound healing. *J Surg Res* 2012;**176**:343-7.
41. Wenzhao L, Jiangdong N, Deye S, Muliang Ding, Junjie Wang, Xianzhe Huang, et al. Dual regulatory roles of HMGB1 in inflammatory reaction of chondrocyte cells and mice [published correction appears in Cell Cycle. 2020 Apr 10 *Cell Cycle* 2019;**18**(18):2268-80.
42. Wilgus TA, DiPietro LA. Complex roles for VEGF in dermal wound healing. *J Invest Dermatol* 2012;**12**:493-4.
43. Stockmann C, Kirmse S, Helfrich I, Weidemann A, Takeda N, Doedens A, et al. A wound size-dependent effect of myeloid cell-derived vascular endothelial growth factor on wound healing. *J Invest Dermatol* 2011;**131**:797-801.
44. Werner S, Grose R. Regulation of wound healing by growth factors and cytokines. *Phys Rev* 2003;**83**:835-70.
45. Ashcroft GS, Jeong MJ, Ashworth JJ, Hardman M, Jin W, Moutsopoulos N, et al. TNF α is a therapeutic target for impaired cutaneous wound healing. *Wound Rep Reg* 2012;**20**:38-49.
46. Mateo RB, Reichner JS, Albina JE. Interleukin-6 activity in wounds. *Am J Physiol* 1994;**266**:R1840-4.
47. AS MacLeod, Mansbridge JN. The innate immune system in acute and chronic wounds. Critical review. *Adv Wound Care* 2016;**5**:65-78.
48. Robertson FM, Pellegrini AE, Ross MR, Oberyszyn AS, Boros LG, Bijur GN, et al. Interleukin-1 a gene expression during wound healing. *Wound Rep Reg* 1995;**3**:473-84.
49. Jiang T, Tian F, Zheng H, Whitman SA, Lin Y, Zhang Z, et al. Nrf2 suppresses lupus nephritis through inhibition of oxidative injury and the NF- κ B-mediated inflammatory response. *Kidney Int* 2014 Feb;**85**(2):333-43 Epub 2013 Sep 11.

50. Furue M. Regulation of filaggrin, loricrin, and involucrin by IL-4, IL-13, IL-17A, IL-22, AHR, and NRF2: pathogenic implications in atopic dermatitis. *Int J Mol Sci* 2020 Jul 29;21(15):5382.
51. Ding M, Li M, Zhang EM, Yang HL. FULLEROL alleviates myocardial ischemia-reperfusion injury by reducing inflammation and oxidative stress in cardiomyocytes via activating the Nrf2/HO-1 signaling pathway. *Eur Rev Med Pharmacol Sci* 2020 Sep;24(18):9665-74.
52. Li T, Xiao L, Yang J, Ding M, Zhou Z, LaConte L, et al. Trimetallic nitride endohedral fullerenes carboxyl-Gd3N@C80: a new theranostic agent for combating oxidative stress and resolving inflammation. *ACS Appl Mater Interfaces* 2017 May 31;9(21):17681-7.
53. Godwin JW, Pinto AR, Rosenthal NA. Macrophages are required for adult salamander limb regeneration Jun 4 *Proc Natl Acad Sci USA* 2013; 110(23):9415-20, <https://doi.org/10.1073/pnas.1300290110> Epub 2013 May 20. PMID: 23690624; PMCID: PMC3677454.
54. Kuklin AI, Rogachev AV, Soloviov DV, Ivankov OI, Kovalev YS, Utrobin PK, et al. Neutronographic investigations of supramolecular structures on upgraded small-angle spectrometer YuMO. *J Phys Conf Ser* 2017;848012010.
55. Soloviev AG, Solovjeva TM, Ivankov OI, Soloviov DV, Rogachev AV, Kuklin AI. SAS program for two-detector system: seamless curve from both detectors. *J Phys: Conf Ser* 2017;848012020.
56. Molchanova VI, Chikalovets IV, Chernikov OV, Krivoshapko ON, Lukianov PA. Comparative study of the biological activity of bioglycans from the far eastern mussel *crenomytilus grayanus*. *Pacific Med J* 2012; 1:47-50 (in Russian).
57. Livak KJ, Schmittgen TD. Analysis of relative gene expression data using real-time quantitative PCR and the $2^{-\Delta\Delta C(T)}$ method. *Methods* 2001;25(4):402-8.